POLITECNICO DI TORINO
Repository ISTITUZIONALE

A Novel Model Reference Adaptive Control Approach for Three-Phase Inverter Applications

Original
A Novel Model Reference Adaptive Control Approach for Three-Phase Inverter Applications / Ahmed Qureshi, M., Torelli, F., Stella, F., Musumeci, S., Mazza, A., Chicco, G.. - In: IEEE JOURNAL OF EMERGING AND SELECTED TOPICS IN POWER ELECTRONICS. - ISSN 2168-6777. - (2026). [10.1109/JESTPE.2025.3584899]

Availability:
This version is available at: 11583/3004805 since: 2025-11-04T13:59:09Z

Publisher:
IEEE

Published
DOI:10.1109/JESTPE.2025.3584899

Terms of use:

This article is made available under terms and conditions as specified in the corresponding bibliographic description in the repository

Publisher copyright
IEEE postprint/Author's Accepted Manuscript

©2026 IEEE. Personal use of this material is permitted. Permission from IEEE must be obtained for all other uses, in any current or future media, including reprinting/republishing this material for advertising or promotional purposes, creating new collecting works, for resale or lists, or reuse of any copyrighted component of this work in other works.

(Article begins on next page)

26 November 2026

This article has been accepted for publication in IEEE Journal of Emerging and Selected Topics in Power Electronics. This is the author's version which has not been fully edited and content may change prior to final publication. Citation information: DOI 10.1109/JESTPE.2025.3584899

A Novel Model Reference Adaptive Control Approach for Three-Phase Inverter Applications

Muhammad Ahmed Qureshi, *Graduate Student Member, IEEE,* Francesco Torelli, Fausto Stella, *Member, IEEE,* Salvatore Musumeci, *Member, IEEE,* Andrea Mazza, *Senior Member, IEEE,* and Gianfranco Chicco, *Fellow, IEEE*

***Abstract*—This paper presents an innovative control strategy for three-phase inverters. The proposed model reference adaptive control utilizes the Torelli Control Box (TCB) methodology, previously applied successfully to DC-DC converters, to regulate a three-phase inverter without load current sensors. This direct control approach overcomes the limitations of using traditional dual-loop control methodologies based on linear control systems and offers a robust solution against non-linearities and system disturbances. This paper formulates the overall framework for using the TCB method to control three-phase inverters. The performance of the TCB method is compared with linear and non-linear control strategies proposed in the literature, demonstrating the relative advantages in managing three-phase inverter complexities. The results have been verified in the laboratory on an experimental three-phase inverter installation that supplies a resistive load, with the proposed controller implemented in a microcontroller.**

***Index Terms*—Lyapunov theory; power converter; regulation; sensitivity theory; Torelli Control Box; three-phase inverter.**

I. Introduction

THREE-phase inverters are essential components in contemporary electrical systems, serving as the bridge between direct current (DC) and alternating current (AC). The applications of three-phase inverters are diverse and far-reaching. In manufacturing and processing plants, these inverters are crucial for driving AC motors, enabling precise control over speed and torque in applications like conveyors, pumps, fans, and compressors. Moreover, three-phase inverters are vital components in Uninterruptible Power Supply (UPS) systems, providing reliable AC power during grid failures to critical equipment in medical facilities, data centers, and communication systems [1]. Similarly, commercial and residential buildings increasingly rely on three-phase inverters to control compressors and fans, optimizing comfort levels and energy efficiency [2]. In the mobility sector, these inverters play a crucial role in electric trains and trams, and convert DC voltage from batteries to AC for electric motor operation in EVs and hybrid vehicles. One of the most significant contributions of three-phase inverters refers to interfacing renewable energy systems with the grid, for solar photovoltaic (PV) systems and wind energy systems.

M.A. Qureshi, F. Stella, S. Musumeci, A. Mazza and G. Chicco are with the Dipartimento Energia "Galileo Ferraris", Politecnico di Torino, corso Duca degli Abruzzi 24, 10129 Torino, Italy (email: muhammad.qureshi@polito.it, fausto.stella@polito.it, salvatore.musumeci@polito.it, andrea.mazza@polito.it, gianfranco.chicco@polito.it).

F. Torelli is with Politecnico di Bari, via Orabona 4, 70125 Bari, Italy.

Manuscript received ... 2025; revised ... 2025.

In the literature, various control strategies for Pulse Width Modulation (PWM) converters have been introduced aiming to achieve high power factor and low total harmonic distortion (THD) in the input line currents. Some linear control strategies proposed include:

- Phase and Amplitude Control (PAC) [3], [4], effective in reducing steady-state current harmonics and output voltage ripple but introduces a DC current component on the AC side, negatively impacting the DC load current and voltage during transients.
- Hysteresis Current Control (HCC) [5], [6], which offers fast dynamic response, high accuracy, no DC offset, and strong robustness. However, its average switching frequency varies with the DC load current, leading to uneven and random switching patterns that impose additional stress on the switching devices.
- Predicted Current Control with Fixed Switching Frequency (PCFF) [7], which provides a fast dynamic response and a consistent switching pattern, which reduces stress on switching devices, but it is sensitive to parameter variations.

These control strategies along with other linear control techniques offer a range of benefits and drawbacks ranging from complexity of the control circuit, switching frequencies, and complications in transient responses. One common drawback among all the linear approaches is their inability to ensure system stability during large-signal disturbances. The state-space-averaged models of PWM inverters, derived using these strategies, are known to be nonlinear systems. Due to the challenges associated with controlling such nonlinear systems, much of the previous research has focused on applying linear control theory to small-signal linearized models of these DC-AC converters. However, these control laws typically only ensure system stability for small perturbations around the operating points of both state and input variables. Therefore, it is highly desirable to develop control strategies that can aim at global stability for the converter without resorting to linearization of its mathematical model.

Different nonlinear control strategies have also been proposed to provide an improved response from the system. One of the frequently adopted techniques is the Model Predictive Control (MPC) used for the regulation of a three-phase inverter [8], [9], [10]. While an MPC is simple to implement, it is computationally demanding and its results do not show exceptional performance in terms of steady-state error and THD even when augmented with a current observer. Additionally,

Authorized licensed use limited to: Politecnico di Torino. Downloaded on January 15,2026 at 08:57:10 UTC from IEEE Xplore. Restrictions apply.
© 2025 IEEE. All rights reserved, including rights for text and data mining and training of artificial intelligence and similar technologies. Personal use is permitted, but republication/redistribution requires IEEE permission. See https://www.ieee.org/publications/rights/index.html for more information.

This article has been accepted for publication in IEEE Journal of Emerging and Selected Topics in Power Electronics. This is the author's version which has not been fully edited and content may change prior to final publication. Citation information: DOI 10.1109/JESTPE.2025.3584899

MPC relies on the knowledge of the system parameters, which can be a limitation.

Another control approach is based on deadbeat controller. While it provides an appropriate response during transients, its performance is highly dependent on model uncertainties and parameter perturbations [11], [12]. The controller tends to become unstable if the parameters are not known exactly.

Unlike the deadbeat control approach, H_∞ controllers are based on robust control theory and are capable of handling system uncertainties. Nevertheless, the controllers generated are often too intricate for digital processors due to their high order [13]. To address this point, a suitable order reduction process is necessary to create a manageable controller, but this process may compromise the characteristics of the original controller. Additionally, the design specifications of these methods, including weighting functions and perturbation models, are complex, which can be seen as another disadvantage.

Another method is based on feedback-linearization approach [14]. The controller is able to obtain adequate total harmonic distortion results for both linear and nonlinear loads but it does not take into account the control performance under parametric uncertainties.

Lyapunov-based approaches are based on the use of Lyapunov energy function. Among the traditional Lyapunov-based control approaches, Sliding Mode Control (SMC)-based methodologies have been widely applied for the regulation of three-phase inverters [15], [16]. SMC is used because it is capable of providing protection against parametric uncertainties and offer a robust response in dynamic conditions. However, the drawback of SMC is that it suffers from time-varying frequency and chattering phenomenon.

Lyapunov-based methods have been used for the regulation of a rectifier [17] and an active filter [18]. In the derivation of this approach, it is ensured that the derivative of the Lyapunov function is negative under all possible operating conditions. However, this approach suffers from considerable steady state error and large THD in the output voltage. This method has been recently improved in [1] by the introduction of output voltage feedback loops. This results in considerable mitigation of steady-state errors and improvement in reducing the harmonics in the output voltage. In [1] the performance of the method proposed is successfully compared against deadbeat and SMC controllers presented in the literature. Due to the excellent performance of this controller, it is used as a benchmark for further comparisons.

This paper presents an innovative control strategy for a three-phase voltage source inverter, with an output LC filter, that supplies a resistive three-phase load. This strategy is based on a closed-loop controller that adapts its characteristics to follow a reference trajectory defined on the basis of the model of the system. The corresponding Model Reference Adaptive Control (MRAC) minimizes the error between the output and the reference through an adaptation mechanism that implements the concepts of the Torelli Control Box (TCB) approach [19], so that the error on the output variable has an asymptotic convergence to zero. The TCB approach consists of a computational paradigm based on the Lyapunov theory and the sensitivity theory, which has already been successfully used in applications to different domains, from power system optimization [20] to the control of Buck and Boost DC/DC converters [21].

The original contributions of this paper are:

- The formulation, for the first time, of a MRAC-TCB approach to control a three-phase inverter. The proposed approach allows the system to reach global asymptotic stability without linearization. Furthermore, the proposed controller provides a fixed frequency and low-cost solution as it does not require the use of current sensors.
- The description of the characteristics and effectiveness of the proposed MRAC-TCB approach applied to simulated cases of a three-phase voltage-source inverter that serves a resistive load, operated under balanced and unbalanced conditions, including comparisons with other types of controllers.
- The experimental verification of the robustness of the MRAC-TCB control on a three-phase inverter prototype, with the controller implemented in a microcontroller, again compared with a traditional controller.

The next sections of this paper are organized as follows. Section II illustrates the conceptual framework of the proposed methodology. Section III presents the mathematical model of the three phase inverter system used for the application of the MRAC-TCB control approach. Section IV shows the simulation results, followed by the experimental results in Section V and by the conclusions drawn in Section VI.

II. Conceptual Framework

A. Formulation of the TCB Approach for Model Reference Adaptive Control

Let us consider a non-linear differential-algebraic equation system in which the state variable vector $\mathbf{x}(t) \in \mathbb{R}$, the control variable vector $\mathbf{u}(t) \in \mathbb{R}$ and the vector $\mathbf{y}(t) \in \mathbb{R}$ of the algebraic variables depend on time t, as follows:

$$\dot{\mathbf{x}}(t) = \mathbf{f}(\mathbf{x}(t), \mathbf{u}(t)) \tag{1}$$

$$\mathbf{g}(\mathbf{x}(t)) - \mathbf{y}(t) = \mathbf{0} \tag{2}$$

Equations (1) and (2) represent the derivative in time of the state variables and the algebraic equations, respectively.

The basic idea of the TCB-based control approach is the adaptive stabilization of non-linear systems. The most important design specification is to achieve asymptotic tracking of a known reference trajectory with the strongest possible form of stability. In addition, the adaptive controller provides effective means for shaping the transient performance and thus allows different performance-robustness trade-offs. The suggested approach is composed of three steps:

1) Formulation of the tracking error of the output, where the output is coincident with the state variable of interest, and of the reference model expressed by a desired trajectory $\mathbf{y}(t)$.
2) Evaluation of system equilibrium point involving the steady state $\mathbf{x}^*$ of the system and the corresponding input signal $\mathbf{u}^*$.
3) Design of the control law which forces the system trajectory to reach asymptotically the prefixed equilibrium

Authorized licensed use limited to: Politecnico di Torino. Downloaded on January 15,2026 at 08:57:10 UTC from IEEE Xplore. Restrictions apply.
© 2025 IEEE. All rights reserved, including rights for text and data mining and training of artificial intelligence and similar technologies. Personal use is permitted, but republication/redistribution requires IEEE permission. See https://www.ieee.org/publications/rights/index.html for more information.

This article has been accepted for publication in IEEE Journal of Emerging and Selected Topics in Power Electronics. This is the author's version which has not been fully edited and content may change prior to final publication. Citation information: DOI 10.1109/JESTPE.2025.3584899

point by following the computational paradigm based on Lyapunov theory and sensitivity theory.

The reference trajectory is used to specify the ideal response of the adaptive control system to the external change. The choice of the reference model should reflect some performance specifications such as rise time, settling time, overshoot, or frequency domain characteristics. In the sequel, the time argument is omitted for brevity. The output reference model dynamics are usually expressed by a low-order linear system as follows:

$$\ddot{y} + k_1\dot{y} + k_0 y = k_0 y_{\mathrm{d}} \tag{3}$$

where the parameters k_1 and k_2 are chosen so that the polynomial $P(s) = s^2 + k_1 s + k_0$ is an Hurwitz polynomial and y_{d} is the steady state of the output signal.

In the second step, the reference trajectories of the state variables **x** and the control signals **u** are evaluated in the (**x**,**u**) composite domain. Let us impose $y = x_i$, where x_i is the state variable of interest. The reference trajectories in the domain (**x**,**u**) are obtained by the steady-state conditions of the system expressed in (1) and (2):

$$\mathbf{f}(\mathbf{x}, \mathbf{u}) = \mathbf{0} \tag{4}$$

$$x_i - y = 0 \tag{5}$$

Consequently, the trajectories are characterized, for each y, by the equilibrium points of the dynamic system. The region described by the trajectories assumes the characteristics of an attraction domain, for the system (1), coincident with the entire state space. The solution of (4) and (5) can be re-proposed in the evaluation of the equilibrium point (**x***,**u***) that minimizes the error functions:

$$\mathbf{e}_1 = \mathbf{f}(\mathbf{x}, \mathbf{u}) \tag{6}$$

$$e_2 = x_i - y \tag{7}$$

Let $\mathbf{e} = [\mathbf{e}_1^{\mathrm{T}}, e_2]^{\mathrm{T}}$ and $\mathbf{z} = [\mathbf{x}^{\mathrm{T}}, \mathbf{u}^{\mathrm{T}}]^{\mathrm{T}}$. Minimizing **e** means minimizing the following quadratic function:

$$\Psi = \frac{1}{2}\mathbf{e}^{\mathrm{T}}\mathbf{e} \tag{8}$$

The traditional approach for finding the minimum of (8) consists of solving the following first-order derivative condition:

$$\frac{\partial \Psi(\mathbf{z})}{\partial \mathbf{z}} = \frac{\partial \mathbf{e}(\mathbf{z})}{\partial \mathbf{z}}\mathbf{e}(\mathbf{z}) = 0 \tag{9}$$

Due to the non-linear nature of the resulting equations, numerical methods are usually adopted to obtain a solution within a prefixed tolerance.

In the third step, the adaption mechanism suggested in the TCB method is explicitly designed so that the asymptotic stability of the equilibrium point is guaranteed. The adaptation mechanism design is based on the minimization of the following tracking errors with respect to control signal **u**:

(10)

where $\mathbf{W_x}$ and $\mathbf{W_u}$ are diagonal matrices that contain the positive weights associated to each error referring to the state variables **x** and control variables **u**, respectively. The term **f**(**x***,**u***) is null as it is estimated in an equilibrium point of the system.

Assuming $\mathbf{e} = [\mathbf{e_x}^{\mathrm{T}}, \mathbf{e_u}^{\mathrm{T}}, \mathbf{e_f}^{\mathrm{T}}]^{\mathrm{T}}$, since the state vector **x** is **u**-dependent, the controller design problem can be recast as follows:

$$\dot{\mathbf{x}}(\mathbf{u}) = \mathbf{f}(\mathbf{x}(\mathbf{u}), \mathbf{u}) \tag{11}$$

$$\mathbf{e}(\mathbf{x}(\mathbf{u}), \mathbf{u}) = \mathbf{0} \tag{12}$$

Therefore, the problem consists of evaluating the input vector **u**(t) such that each component of the error vector **e** is reduced to zero while simultaneously fulfilling the dynamic constraint given by (11).

The controller design problem is converted in a multi-objective optimization problem with dynamic constraint. Let us consider the composite vector $\mathbf{e}(\mathbf{x}(\mathbf{u}), \mathbf{u})$ as a unique function of **u**, with $\mathbf{e}(\mathbf{x}(\mathbf{u}), \mathbf{u}) = \mathbf{0}$ at **u** = **u***. Therefore, the goal is to change **u** until $\mathbf{e}(\mathbf{x}(\mathbf{u}), \mathbf{u})$ is either zero or minimal.

A possible way to achieve this goal is based on the definition of the following candidate Lyapunov function:

$$V = \frac{1}{2}\mathbf{e}^{\mathrm{T}}\mathbf{e} \tag{13}$$

that is a positive semi-definite scalar function.

Conceptually, if the time derivative $\dot{V}$ can be made negative definite or negative semi-definite, then $\mathbf{e}(\mathbf{u})$ approaches the minimum of **e** asymptotically. By determining $\dot{V}$ from (12) :

$$\dot{V} = \mathbf{e}^{\mathrm{T}}\dot{\mathbf{e}} \tag{14}$$

and because

$$\dot{\mathbf{e}} = \frac{\partial \mathbf{e}}{\partial \mathbf{u}}\dot{\mathbf{u}} \tag{15}$$

it results

$$\dot{V} = \mathbf{e}^{\mathrm{T}}\frac{\partial \mathbf{e}}{\partial \mathbf{u}}\dot{\mathbf{u}} \tag{16}$$

A key point of the TCB approach is to impose the condition that $\dot{\mathbf{u}}$ changes according to the gradient of *V*, that is:

$$\dot{\mathbf{u}} = -K\Big(\frac{\partial V}{\partial \mathbf{u}}\Big)^{\mathrm{T}} = -K\Big(\frac{\partial \mathbf{e}}{\partial \mathbf{u}}\Big)^{\mathrm{T}}\mathbf{e} \tag{17}$$

where the gradient is again defined as a row vector and *K* is a positive constant.

Then, by substituting (16) into (15) and (14), it follows:

$$\dot{V} = -K\mathbf{e}^{\mathrm{T}}\Big(\frac{\partial \mathbf{e}}{\partial \mathbf{u}}\Big)\Big(\frac{\partial \mathbf{e}}{\partial \mathbf{u}}\Big)^{\mathrm{T}}\mathbf{e} \tag{18}$$

$$\dot{\mathbf{e}} = -K\Big(\frac{\partial \mathbf{e}}{\partial \mathbf{u}}\Big)\Big(\frac{\partial \mathbf{e}}{\partial \mathbf{u}}\Big)^{\mathrm{T}}\mathbf{e} \tag{19}$$

Equation (18) is a quadratic form that is certainly negative semi-definite.

The foregoing mathematical manipulation indicates that to guarantee the asymptotic stability of the equilibrium point **u***, the control action **u** must be generated according to the formulation defined by (16). This leads to satisfy both conditions ($V(\mathbf{e}) > 0$ and $\dot{V}(\mathbf{e}) < 0$) associated to the Lyapunov theory.

In addition, by observing (19) it has to be noticed that the matrix $\left(\frac{\partial \mathbf{e}}{\partial \mathbf{u}}\right)\left(\frac{\partial \mathbf{e}}{\partial \mathbf{u}}\right)^{\mathrm{T}}$ is positive definite and symmetric, and its eigenvalues are real and positive. Hence, it can be concluded that **e**(**x**,**u**) exponentially converges to the equilibrium point **e**(**x***,**u***) = **0** which implies **x** = **x***, **u** = **u*** and **f**(**x**,**u**) = **f**(**x***,**u***) = **0**.

Authorized licensed use limited to: Politecnico di Torino. Downloaded on January 15,2026 at 08:57:10 UTC from IEEE Xplore. Restrictions apply.
© 2025 IEEE. All rights reserved, including rights for text and data mining and training of artificial intelligence and similar technologies. Personal use is permitted, but republication/redistribution requires IEEE permission. See https://www.ieee.org/publications/rights/index.html for more information.

This article has been accepted for publication in IEEE Journal of Emerging and Selected Topics in Power Electronics. This is the author's version which has not been fully edited and content may change prior to final publication. Citation information: DOI 10.1109/JESTPE.2025.3584899

The vector $\partial \mathbf{e}/\partial \mathbf{u}$ can be expressed as follows:

$$\frac{\partial \mathbf{e}}{\partial \mathbf{u}} = \left[\left(\frac{\partial \mathbf{x}}{\partial \mathbf{u}}\right)^{\mathrm{T}}, \mathbf{I}, \left(\frac{\partial \mathbf{f}}{\partial \mathbf{x}}\frac{\partial \mathbf{x}}{\partial \mathbf{u}} + \frac{\partial \mathbf{f}}{\partial \mathbf{u}}\right)^{\mathrm{T}}\right]^{\mathrm{T}} \tag{20}$$

where $\frac{\partial \mathbf{x}}{\partial \mathbf{u}}$ is the sensitivity vector that is achieved as the solution of the state sensitivity differential equations obtained deriving the system equation (1) with respect to $\mathbf{u}$:

$$\frac{\partial \dot{\mathbf{x}}}{\partial \mathbf{u}} = \frac{\partial \mathbf{f}}{\partial \mathbf{x}}\frac{\partial \mathbf{x}}{\partial \mathbf{u}} + \frac{\partial \mathbf{f}}{\partial \mathbf{u}} \tag{21}$$

In conclusion, the TCB controller design is obtained by solving the sensitivity equation in (21), together with the differential equations (1), (3), and

$$\dot{\mathbf{u}} = -K\left[\left(\frac{\partial \mathbf{x}}{\partial \mathbf{u}}\right)^{\mathrm{T}}(\mathbf{x}-\mathbf{x}^*) + \mathbf{I}(\mathbf{u}-\mathbf{u}^*) + \frac{\partial \mathbf{f}}{\partial \mathbf{x}}\frac{\partial \mathbf{x}}{\partial \mathbf{u}} + \frac{\partial \mathbf{f}}{\partial \mathbf{u}}^{\mathrm{T}}\mathbf{f}(\mathbf{x},\mathbf{u})\right] \tag{22}$$

B. Discussion on the Adaptive Control Properties of the TCB Approach

In principle, the TCB control aims at following the reference trajectory of the desired output, which can be either a steady-state value or a trajectory that includes transients. Because of the adaptive nature of the TCB control, the output variable follows only the dynamics of the reference trajectory and is insensitive to model uncertainties or parametric variations [21]. In case of setting up a transient reference trajectory, the dynamics of the controller have to be significantly faster than the dynamics of the reference transient. In this way, setting up the gain of the controller high enough to make the output variable of the system approaching fast the reference transient trajectory, the performance of the TCB control is remarkably robust according to its mathematical formulation.

During time, the response evolves in the direction of the reference trajectory to reduce the error with respect to the reference trajectory itself, and becomes practically insensitive to noise in the input variables. The only case in which the measurement noise can affect the controller performance is in the presence of noise in the measured output variable to be compared with the reference trajectory. In this case, the response can be less regular when approaching the reference trajectory because of the biased or erroneous reporting of the measured value, however, the controller works properly.

III. Application of an Observer-Based MRAC-TCB Approach to Three-phase Voltage Controlled Inverter

A. Three-phase Inverter Modeling

Fig. 1 depicts a three-phase inverter with LC filter. The mathematical model in the synchronously rotating dq frame can be expressed as follows:

$$\begin{cases} \dot{x}_1 &= \frac{1}{L}(\frac{\mu_d V_s}{2} - Rx_1 - x_3 + \omega L x_2) \\ \dot{x}_2 &= \frac{1}{L}(\frac{\mu_q V_s}{2} - Rx_2 - x_4 - \omega L x_1) \\ \dot{x}_3 &= \frac{1}{C}(x_1 - i_{od} + \omega C x_4) \\ \dot{x}_4 &= \frac{1}{C}(x_2 - i_{oq} - \omega C x_3) \end{cases} \tag{23}$$

where x_1, x_2 are the three-phase inductor currents expressed in the dq frame (i.e. i_{Ld} and i_{Lq}), while x_3 and x_4 are the output voltages (v_{od} and v_{oq}, respectively). Similarly, u_d and u_q are the dq representation of the three-phase duty cycle. The terms L, C and R are the inductance, capacitance, and inductor resistance values of the converters, respectively. Moreover, ω is the angular frequency, i_{od} and i_{oq} are the load currents in the dq domain, and the load is represented by the resistance R_L.

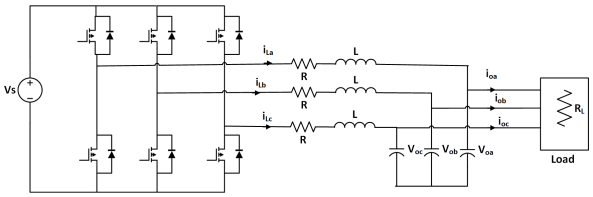


Fig. 1. Three-phase inverter with LC filter.

B. Adaptive State Observer Design for the Three-phase Inverter

For this application of the MRAC-TCB approach, a state observer is used to estimate the unknown load resistance under dynamic conditions. State observers to estimate the load have previously been used for DC-DC boost converters in [22] and [23].

For the design of the observer, both the inductor current and the output voltage are considered accessible. The observer is designed to estimate the value of the unknown load resistance R_L. Considering $1/R_L$ as θ, the following estimator equations can be written for the three-phase observer:

$$\begin{cases} \dot{\hat{x}}_1 &= \frac{1}{L}(\frac{\mu_d V_s}{2} - R\hat{x}_1 - \hat{x}_3 + \omega L \hat{x}_2) + K_1(x_1 - \hat{x}_1) \\ \dot{\hat{x}}_2 &= \frac{1}{L}(\frac{\mu_q V_s}{2} - R\hat{x}_2 - \hat{x}_4 - \omega L \hat{x}_1 + K_2(x_2 - \hat{x}_2) \\ \dot{\hat{x}}_3 &= \frac{1}{C}(\hat{x}_1 - x_3\hat{\theta} + \omega C \hat{x}_4) + K_3(x_3 - \hat{x}_3) \\ \dot{\hat{x}}_4 &= \frac{1}{C}(\hat{x}_2 - x_4\hat{\theta} - \omega C \hat{x}_3) + K_4(x_4 - \hat{x}_4) \end{cases} \tag{24}$$

where $\hat{x}_1$, $\hat{x}_2$, $\hat{x}_3$ and $\hat{x}_4$ are the estimates of their respective state variables, K_1 to K_4 are observer gains, and $\hat{\theta}$ is the estimate of θ.

The next step is to design an adaptation law for $\hat{\theta}$. Let us start by defining the following state error terms:

$$\begin{cases} \tilde{x}_1 = x_1 - \hat{x}_1 \\ \tilde{x}_2 = x_2 - \hat{x}_2 \\ \tilde{x}_3 = x_3 - \hat{x}_3 \\ \tilde{x}_4 = x_4 - \hat{x}_4 \end{cases} \tag{25}$$

together with

$$\tilde{\theta} = \theta - \hat{\theta} \tag{26}$$

Using (23) and (24) results in the following formulation:

$$\begin{cases} \dot{\tilde{x}}_1 &= \frac{1}{L}(-R\tilde{x}_1 - \tilde{x}_3 + \omega L \tilde{x}_2) - K_1\tilde{x}_1 \\ \dot{\tilde{x}}_2 &= \frac{1}{L}(-R\tilde{x}_2 - \tilde{x}_4 - \omega L \tilde{x}_1) - K_2\tilde{x}_2 \\ \dot{\tilde{x}}_3 &= \frac{1}{C}(\tilde{x}_1 - x_3\tilde{\theta} + \omega C \tilde{x}_4) - K_3\tilde{x}_3 \\ \dot{\tilde{x}}_4 &= \frac{1}{C}(\tilde{x}_2 - x_4\tilde{\theta} - \omega C \tilde{x}_3) - K_4\tilde{x}_4 \end{cases} \tag{27}$$

To find the adaptive law for $\hat{\theta}$, let us consider the following Lyapunov function:

$$V = \frac{1}{2}L\tilde{x}_1^2 + \frac{1}{2}L\tilde{x}_2^2 + \frac{1}{2}C\tilde{x}_3^2 + \frac{1}{2}C\tilde{x}_4^2 + \frac{1}{2}\gamma\tilde{\theta}^2 \tag{28}$$

Authorized licensed use limited to: Politecnico di Torino. Downloaded on January 15,2026 at 08:57:10 UTC from IEEE Xplore. Restrictions apply.
© 2025 IEEE. All rights reserved, including rights for text and data mining and training of artificial intelligence and similar technologies. Personal use is permitted, but republication/redistribution requires IEEE permission. See https://www.ieee.org/publications/rights/index.html for more information.

This article has been accepted for publication in IEEE Journal of Emerging and Selected Topics in Power Electronics. This is the author's version which has not been fully edited and content may change prior to final publication. Citation information: DOI 10.1109/JESTPE.2025.3584899

where γ is a design parameter. The time derivative of the Lyapunov function is expressed as follows:

$$\begin{aligned}\dot{V} = &-K_1\tilde{x}_1^2 - K_2\tilde{x}_2^2 - K_3\tilde{x}_3^2 - K_4\tilde{x}_4^2 \\ &+\tilde{\theta}(-\tilde{x}_3x_3 - \tilde{x}_4x_4 + \gamma\ \dot{\tilde{\theta}}) + \epsilon(\mathbf{x}, \tilde{\mathbf{x}})\end{aligned} \tag{29}$$

The adaptation law for $\tilde{\theta}$ is determined by the following equation:

$$\dot{\hat{\theta}} = -\gamma(x_3\tilde{x}_3 + x_4\tilde{x}_4) \tag{30}$$

The function $\epsilon(\mathbf{x}, \tilde{\mathbf{x}})$ is such that when the adaptive TCB control law derives the state variables $\mathbf{x}$ to $\hat{\mathbf{x}}$, the function goes to zero and the Lyapunov function is negative definite.

C. MRAC-TCB Design

As indicated in Section II-A, the MRAC-TCB approach is implemented through three distinct steps:

1) First step: The reference model is generated as a reference signal to regulate the output of the converter. This reference signal is the desired value of v_{od} and v_{oq}, denoted as y_{od} and y_{oq}, respectively. The state variable vector $\mathbf{x}$ includes x_1, x_2, x_3, and x_4, the control variable vector $\mathbf{u}$ contains u_d and u_q, and the algebraic variable $\mathbf{y}$ contains y_{od} and y_{oq}.

2) Second step: The coordinates of the equilibrium point are determined within the composite domain ($\mathbf{x}$, $\mathbf{u}$), indicated as ($\mathbf{x}$*, $\mathbf{u}$*). To achieve this, the equilibrium point for steady-state values is derived by setting (14) to zero. But due to the adaptive design in which the load resistance is determined using the observer, the load resistance R_L is redefined in terms of $\hat{\theta}$, resulting in the following equations:

$$\begin{cases} x_1^* = y_{od}\hat{\theta} \\ x_2^* = y_{oq}\hat{\theta} + Cy_{od}\omega \\ u_d^* = \frac{2}{V_s}(-CLy_{od}\omega^2 - Ly_{oq}\hat{\theta}\omega + Ry_{od}\hat{\theta} + y_{od}) \\ u_q^* = \frac{2}{V_s}(Ry_{oq}\hat{\theta} + Ly_{od}\hat{\theta}\omega + CRy_{od}\omega) \end{cases} \tag{31}$$

.

3) Third step: The adaptation mechanism is designed for the minimization of the following tracking errors:

$$\begin{cases} e_1 = \alpha_1(x_1 - x_1^*) \\ e_2 = \alpha_1(x_2 - x_2^*) \\ e_3 = \alpha_2(x_3 - x_3^*) \\ e_4 = \alpha_2(x_4 - x_4^*) \\ e_5 = \beta(u_d - u_d^*) \\ e_6 = \beta(u_q - u_q^*) \end{cases} \tag{32}$$

The weight vectors α_1, α_2, and β are determined empirically to adjust the response of the system. Again, using the expression defined in (17) and the error vector mentioned above, the control equation for u_a becomes:

$$\begin{aligned}\dot{u}_d = -K\Big[&\alpha_1^2\frac{de_1}{du_d}e_1 + \alpha_1^2\frac{de_2}{du_d}e_2 + \alpha_2^2\frac{de_3}{du_d}e_3 \\ &+\alpha_2^2\frac{de_4}{du_d}e_4 + \beta^2\frac{de_5}{du_d}e_5 + \beta^2\frac{de_6}{du_d}e_6\Big]\end{aligned} \tag{33}$$

$$\begin{aligned}\dot{u}_q = -K\Big[&\alpha_1^2\frac{de_1}{du_q}e_1 + \alpha_1^2\frac{de_2}{du_q}e_2 + \alpha_2^2\frac{de_3}{du_q}e_3 \\ &+\alpha_2^2\frac{de_4}{du_q}e_4 + \beta^2\frac{de_5}{du_q}e_5 + \beta^2\frac{de_6}{du_q}e_6\Big]\end{aligned} \tag{34}$$

where K is the gain factor with constant value given in Table II.

The derivatives of the error equations in (32) with respect to u_d are given by following equations:

$$\begin{cases} \frac{de_1}{du_d} = \alpha_1(\hat{y}_1 - y_{od}\frac{d\hat{\theta}}{du_d}) \\ \frac{de_2}{du_d} = \alpha_1(\hat{y}_2 - y_{oq}\frac{d\hat{\theta}}{du_d}) \\ \frac{de_3}{du_d} = \alpha_2\hat{y}_3 \\ \frac{de_4}{du_d} = \alpha_2\hat{y}_4 \\ \frac{de_5}{du_d} = \beta(\frac{2}{V_s}(Ly_{oq}\omega\frac{d\hat{\theta}}{du_d} - Ry_{od}\frac{d\hat{\theta}}{du_d}) + 1) \\ \frac{de_6}{du_d} = \beta(\frac{-2}{V_s}(Ry_{oq}\frac{d\hat{\theta}}{du_d} + Ly_{od}\omega\frac{d\hat{\theta}}{du_d})) \end{cases} \tag{35}$$

where $\hat{y}$ is a sensitivity parameter representing $\frac{d\hat{\mathbf{x}}}{du_d}$, and $\hat{\mathbf{y}}$ is calculated from (24) by the following set of equations:

$$\begin{cases} \dot{\hat{y}}_1 &= \frac{1}{L}(\frac{V_s}{2} - R\hat{y}_1 - \hat{y}_3 + \omega L\hat{y}_2) + K_1(y_1 - \hat{y_1}) \\ \dot{\hat{y}}_2 &= \frac{1}{L}(-R\hat{y}_2 - \hat{y}_4 - \omega L\hat{y}_1) + K_2(y_2 - \hat{y}_2) \\ \dot{\hat{y}}_3 &= \frac{1}{C}(\hat{y}_1 - y_3\hat{\theta} + \omega C\hat{y}_4) + K_3(y_3 - \hat{y}_3) \\ \dot{\hat{y}}_4 &= \frac{1}{C}(\hat{y}_2 - y_4\hat{\theta} - \omega C\hat{y}_3) + K_4(y_4 - \hat{y}_4) \end{cases} \tag{36}$$

The sensitivity parameter $\mathbf{y}$ representing $\frac{d\mathbf{x}}{du_d}$ is derived by the following equations:

$$\begin{cases} \dot{y}_1 &= \frac{1}{L}(\frac{V_s}{2} - Ry_1 - y_3 + \omega Ly_2) \\ \dot{y}_2 &= \frac{1}{L}(-Ry_2 - y_4 - \omega Ly_1) \\ \dot{y}_3 &= \frac{1}{C}(y_1 - y_3/R_L + \omega Cy_4) \\ \dot{y}_4 &= \frac{1}{C}(y_2 - y_4/R_L - \omega Cy_3) \end{cases} \tag{37}$$

For the derivation of $\frac{d\hat{\theta}}{du_d}$, using equation (30), the result is:

$$\frac{d\hat{\theta}}{du_d} = -\gamma(y_3\tilde{x}_3 + \tilde{y}_3x_3 + y_4\tilde{x}_4 + \tilde{y}_4x_4) \tag{38}$$

Similarly, for the derivation of equations for the q-domain, the above procedure is repeated.

Again, taking the derivative of (32) with respect to u_q gives the following equations:

$$\begin{cases} \frac{de_1}{du_q} = \alpha_1(\hat{z}_1 - y_{oq}\frac{d\hat{\theta}}{du_q}) \\ \frac{de_2}{du_q} = \alpha_1(\hat{z}_2 - y_{oq}\frac{d\hat{\theta}}{du_q}) \\ \frac{de_3}{du_q} = \alpha_2\hat{z}_3 \\ \frac{de_4}{du_q} = \alpha_2\hat{z}_4 \\ \frac{de_5}{du_q} = \beta(\frac{2}{V_s}(Ly_{oq}\omega\frac{d\hat{\theta}}{du_q} - Ry_{od}\frac{d\hat{\theta}}{du_q})) \\ \frac{de_6}{du_q} = \beta(1 - \frac{2}{V_s}(Ry_{oq}\frac{d\hat{\theta}}{du_q} + Ly_{od}\omega\frac{d\hat{\theta}}{du_q})) \end{cases} \tag{39}$$

For the sensitivity parameter $\hat{z_1}$, using again (24) and finding its derivative against u_q, the following equations are obtained:

$$\begin{cases} \dot{\hat{z}}_1 &= \frac{1}{L}(-R\hat{z}_1 - \hat{z}_3 + \omega L\hat{z}_2) + K_1(z_1 - \hat{z_1}) \\ \dot{\hat{z}}_2 &= \frac{1}{L}(\frac{V_s}{2} - R\hat{z}_2 - \hat{z}_4 - \omega L\hat{z}_1) + K_2(z_2 - \hat{z}_2) \\ \dot{\hat{z}}_3 &= \frac{1}{C}(\hat{z}_1 - z_3\hat{\theta} + \omega C\hat{z}_4) + K_3(z_3 - \hat{z}_3) \\ \dot{\hat{z}}_4 &= \frac{1}{C}(\hat{z}_2 - z_4\hat{\theta} - \omega C\hat{z}_3) + K_4(z_4 - \hat{z}_4) \end{cases} \tag{40}$$

The sensitivity parameter $\mathbf{z}$ representing $\frac{d\mathbf{x}}{du_q}$ is derived by the following equations:

$$\begin{cases} \dot{z}_1 &= \frac{1}{L}(-Rz_1 - z_3 + \omega Lz_2) \\ \dot{z}_2 &= \frac{1}{L}(\frac{V_s}{2} - Rz_2 - z_4 - \omega Lz_1) \\ \dot{z}_3 &= \frac{1}{C}(z_1 - z_3/R_L + \omega Cz_4) \\ \dot{z}_4 &= \frac{1}{C}(z_2 - z_4/R_L - \omega Cz_3) \end{cases} \tag{41}$$

Authorized licensed use limited to: Politecnico di Torino. Downloaded on January 15,2026 at 08:57:10 UTC from IEEE Xplore. Restrictions apply.
© 2025 IEEE. All rights reserved, including rights for text and data mining and training of artificial intelligence and similar technologies. Personal use is permitted, but republication/redistribution requires IEEE permission. See https://www.ieee.org/publications/rights/index.html for more information.

This article has been accepted for publication in IEEE Journal of Emerging and Selected Topics in Power Electronics. This is the author's version which has not been fully edited and content may change prior to final publication. Citation information: DOI 10.1109/JESTPE.2025.3584899

TABLE I
SPECIFICATIONS OF THREE PHASE INVERTER

Description of parameters	Nominal value
Input voltage, V_S	40 V
Reference output voltage, V_{Oref}	24 V (phase-to-phase peak)
Capacitance, C	20 μF
Inductance, L	100 μH
Nominal Load, R	3.3 Ω
Switching frequency, f_s	45 kHz

TABLE II
CONTROLLER GAINS AND OBSERVER GAINS

Description of parameters	Nominal value	Units of Gains
Controller Gain K	5	s^{-1}
α_1	0.25	A^{-1}
α_2	0.050	V^{-1}
β	6.0	-
γ	1.1	J Ω^2
k_1	4.90 x 10^4	s^{-1}
k_2	4.95 x 10^4	s^{-1}
k_3	0.15 x 10^4	s^{-1}
k_4	1.05 x 10^4	s^{-1}

For the derivation of $\frac{d\hat{\theta}}{du_1}$, from (30) it results:

$$\frac{d\hat{\theta}}{du_q} = -\gamma(z_3\tilde{x}_3 + \tilde{z}_3 x_3 + z_4\tilde{x}_4 + \tilde{z}_4 x_4) \tag{42}$$

IV. SIMULATION RESULTS

This section presents the simulation results of the proposed control approach. The parameters used for the three-phase inverter are shown in Table I. The control gains for the TCB controller and the load observer are shown in Table II. It should be noted that the gains are chosen empirically in such a way to achieve an appropriate balance between fast tracking and low overshoot voltage. Generally speaking, the values of the constants K and β are kept one order of magnitude higher than the values of the gains α. The sampling frequency of 45 kHz has been used. No discretization technique has been used for the controller implementation, as the sampling frequency is sufficiently high and the control is sufficiently robust. A dead-time has been added to avoid the risk of short circuits in the inverter. The dead-time compensation solution has been applied following a state-of-the-art approach [24]. Therefore, after compensation, the dead-time does not impact the control loop. The simulations have been performed in the Matlab/Simulink environment.

Fig. 2 shows the block diagram of the observer-based MRAC-TCB control system. As shown in the figure, sensors are used to measure the inductor currents (shown in blue) and capacitor voltages (shown in red). These values are transformed from the phase (abc) domain to the dq domain using the Park transformation. The resulting values of V_{Odq} and I_{Ldq} are then used by the load observer to estimate the load resistor values. Finally, the adaptive TCB controller uses these values to generate μ_d and μ_q. These values are used to derive the six switches S_1 to S_6 after inverse Park transformation to convert μ_d and μ_q to μ_{abc} domain.

The aim is to test the controller's robustness and adaptivity under different scenarios. The first part shows the results when the control system is tested with linear (resistive) load, while the second part shows the response with non-linear loads. The final part shows the comparison of the proposed system with a Sliding Mode Direct Voltage controller taken from the literature [25].

TABLE III
VOLTAGE THD% UNDER DIFFERENT LINEAR LOAD CONDITIONS

Load Resistance R_L (Ω)	THD%
13.20	2.93
6.6	2.52
3.3	2.11
1.65	1.65
0.825	1.48
0.4125	1.20

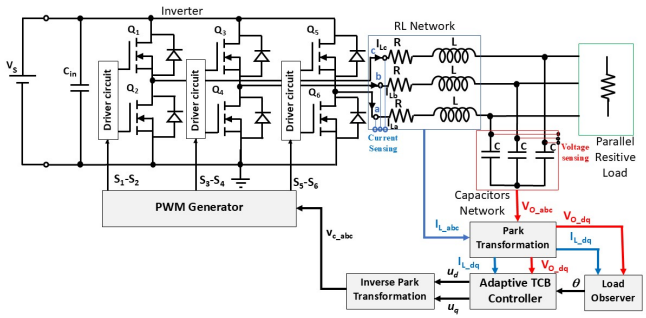


Fig. 2. Proposed scheme of the observer-based TCB adaptive control system.

A. Linear Load

Fig. 3 shows the output phase-to-phase peak voltage of the inverter when the load is halved from R_L = 6.6 Ω to 3.3 Ω and successively to 1.65 Ω at every 0.1 s interval after 0.1 s onwards. The steady state error remains negligible throughout the various load value variations. On average the recovery time is around 5 ms for each step change.

The corresponding $\hat{\theta}$ calculated by the observer is shown in Fig. 4(a), and the load current variation is shown in Fig. 4(b).

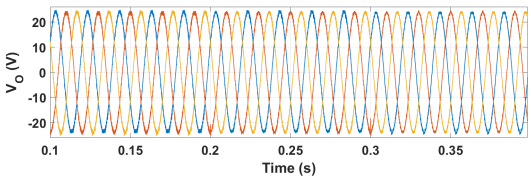


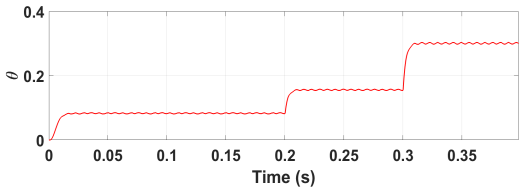
Fig. 3. Output voltage response under linear load variations (phase-to-phase voltage, peak voltage 24 V).

Table III shows the Total Harmonic Distortion (THD) percentage of the voltage at different values of load resistance. As seen from the table, THD% increases from 1.20% for R_L = 0.4125 to 2.93% for R_L = 13.20 Ω.

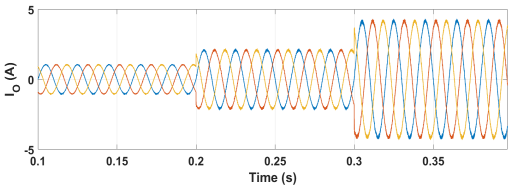
The performance of the controller was next tested under unbalanced load conditions. For this test, phase c was opened at exactly 0.2 s. The corresponding output phase-to-phase voltage and load current are shown in Fig. 5. Fig. 5(b) shows that the current goes to zero at 0.2 s, but as seen from Fig. 5(a), the fault has no significant influence on the phase voltage.

Authorized licensed use limited to: Politecnico di Torino. Downloaded on January 15,2026 at 08:57:10 UTC from IEEE Xplore. Restrictions apply.
© 2025 IEEE. All rights reserved, including rights for text and data mining and training of artificial intelligence and similar technologies. Personal use is permitted, but republication/redistribution requires IEEE permission. See https://www.ieee.org/publications/rights/index.html for more information.

This article has been accepted for publication in IEEE Journal of Emerging and Selected Topics in Power Electronics. This is the author's version which has not been fully edited and content may change prior to final publication. Citation information: DOI 10.1109/JESTPE.2025.3584899

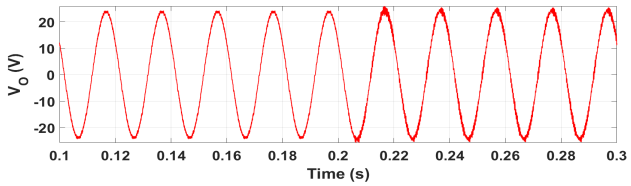


(a)

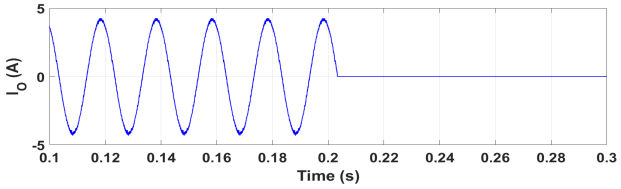


(b)

Fig. 4. (a) Observer output in response to load variations (b) Output current in response to load variations.



(a)



(b)

Fig. 5. (a) Output voltage and (b) Load Current under phase fault conditions.

Finally, a robust control system has also an allowance for parametric uncertainties. Hence, the values of LC parameters have been varied from 50% to 400% of nominal values. Table IV shows the effects of parameter mismatch and its effects on voltage THD% at phase A. As seen from the table, as the values of both L and C increase, the values of the voltage THD% decrease. In the harshest condition, i.e., with L and C reduced to 50% of their nominal values, the maximum THD% of 5.46% is obtained.

TABLE IV
VOLTAGE THD% UNDER INDUCTOR AND CAPACITOR PARAMETER UNCERTAINTIES

Cap. = 10 μF		Cap. = 20 μF		Cap. = 80 μF	
Inductance (μH)	THD %	Inductance (μH)	THD %	Inductance (μH)	THD %
50	5.46	50	1.45	50	0.11
100	2.88	100	2.11	100	1.91
200	1.75	200	1.50	200	1.47
400	1.17	400	1.10	400	1.03

B. Nonlinear Load

The nonlinear load proposed for the testing of the control system is shown in Fig. 6. It is a three-phase diode rectifier with capacitor C_d, inductor L_d and resistance R_L. The values of inductor and capacitor are 100 mH and 20 μF, respectively, while the resistance is changed to different values.

The output voltage and current under nonlinear load are shown in Fig. 7. As seen from Fig. 7(a) for load resistance 13.2 Ω, there is a negligible steady state error, while the output is not as smooth as in the case of the linear load. The THD% of the voltage at phase A is 4.90%, which is below the 8% limit specified by the standard IEEE 519-2014.

The relationship of THD% with the load resistance is shown in Table V. The THD% decreases with the load resistance increase. But even with the lower values of the load resistance, the overall THD% remains within the limit of the standard IEEE 519-2014.

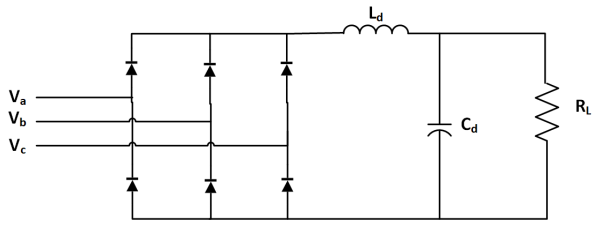
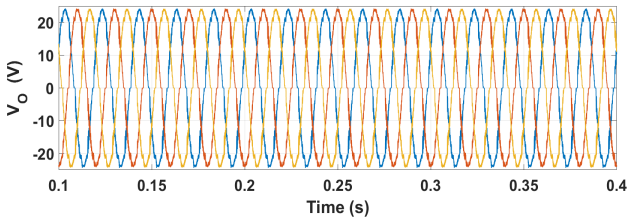


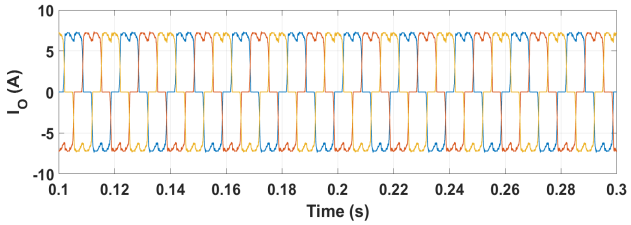
Fig. 6. Three-phase diode rectifier-based nonlinear load.

C. Comparisons with a Cascaded Dual-loop PI Controller and Nonlinear SMDVC Controller Proposed in the Literature

This section presents a comparison between the proposed controller and a Sliding Mode Direct Voltage Loop Controller. The values of the controller constants were fine-tuned to get optimized results. The tests were first carried out in simulation in the Matlab/Simulink environment.



(a)



(b)

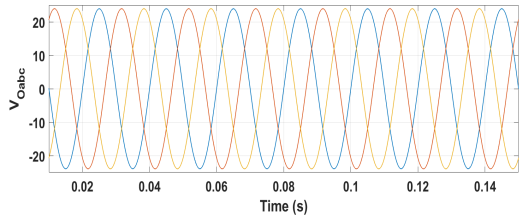
Fig. 7. (a) Output voltage and (b) Load current under nonlinear load.

Authorized licensed use limited to: Politecnico di Torino. Downloaded on January 15,2026 at 08:57:10 UTC from IEEE Xplore. Restrictions apply.
© 2025 IEEE. All rights reserved, including rights for text and data mining and training of artificial intelligence and similar technologies. Personal use is permitted, but republication/redistribution requires IEEE permission. See https://www.ieee.org/publications/rights/index.html for more information.

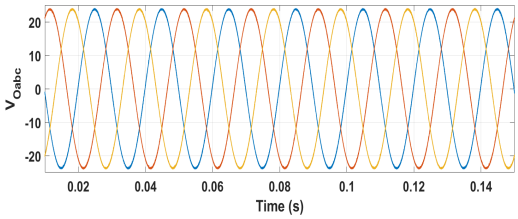
This article has been accepted for publication in IEEE Journal of Emerging and Selected Topics in Power Electronics. This is the author's version which has not been fully edited and content may change prior to final publication. Citation information: DOI 10.1109/JESTPE.2025.3584899

TABLE V
VOLTAGE THD% UNDER DIFFERENT NONLINEAR LOAD CONDITIONS

Load Resistance R_L (Ω)	THD%
3.3	6.71
6.6	5.14
13.2	4.90
30	3.88
50	3.72
75	3.69



(a)



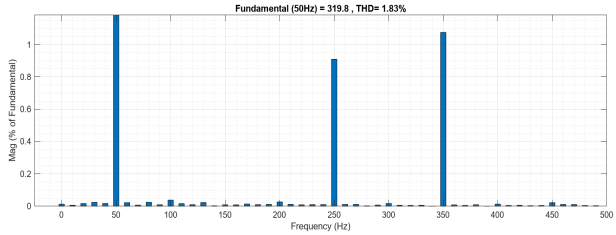
(b)

Fig. 8. (a) Output voltage response of SMDVC under nonlinear load (b) Output voltage response of the cascaded dual-loop PI controller.

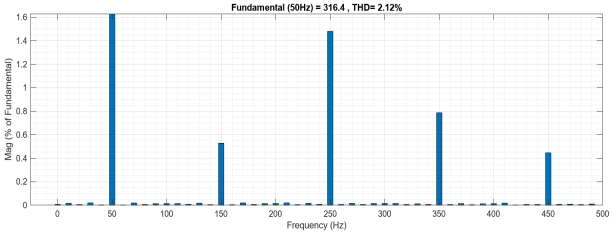
The Sliding Mode Direct Voltage control (SMDVC) is taken from [25]. The performance of the SMDVC controller with three-phase diode bridge rectifier nonlinear load is shown in Fig. 8(a). The SMDVC controller has a smooth output with negligible steady state error. Furthermore, the THD response of the SMDVC controller alongside the proposed controller for load R_L = 70 Ω is shown in Fig. 9. Both controllers show little harmonic distortions. The 5th and 7th harmonics are present for both controllers but their magnitude is mitigated. Overall, the proposed controller (THD of 1.83% as compared to 2.12%) shows slightly improved response in terms of THD percentage. The steady state errors of both controllers are negligible.

As shown in Table VI, our control system does not require the use of load sensors. Apart from the Model predictive controller proposed in [27] which also uses observers, other reported control systems do use sensors for measuring the load current. However, the MPC based controller has a very high computational burden and does not operate on constant frequency like the other approaches.

The feed-forward PI controller is simpler to implement in comparison with other proposed control techniques but it can only guarantee local stability around the operating point. It has also been simulated as shown in Fig. 8(b) and also implemented to obtain the experimental results shown in the next section. Other Lyapunov based control approach and the SMDVC do offer robustness and low steady state errors, but in case of [28] requires the use of additional current sensors. In SMDVC, sensors are used for measuring both inductor and



(a)



(b)

Fig. 9. Phase A voltage THD of (a) TCB-based control system (b) SMDVC controller.

TABLE VI
COMPARISON OF THE PROPOSED CONTROL SYSTEM WITH CONTROL SCHEMES PROPOSED IN THE LITERATURE

Reference	[26]	[27]	[28]	[25]	This paper
Control strategy	Feed-forward PI control	FCS MPC control	Lyapunov function based approach	SMDVC	TCB-based control
Large signal stability guaranteed	No	Not reported	Yes	Yes	Yes
Load current sensors	3	0	3	3	0
Computat. burden	Low	Very high	Medium	Medium	Medium
Switching frequency	Fixed	Varying	Fixed	Fixed	Fixed
THD %	0.48	2.31	1.046	0.19	0.16
Steady-state error %	0.123	3.629	1.046	Negligible	Negligible

load current, and the overall cost is mitigated by designing an observer for estimating the output voltage. However, in practice, it is usually difficult to have access to load current information.

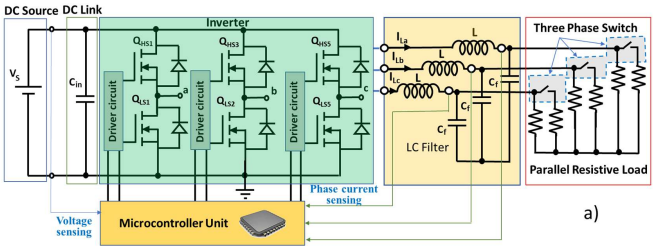
V. EXPERIMENTAL VERIFICATION OF THE RESULTS

A. Testing the Proposed Controller on a Laboratory Prototype

In order to test the validity of the proposed controller in real-time, a prototype of the control system applied to an existing three-phase inverter was built in the laboratory. The experimental setup is shown in Fig. 10. The setup consists of a three-phase MOSFET inverter controlled using a microcontroller. The code that refers to the proposed method has been loaded in the microcontroller using the STM32 Cube IDE program. The filter consists of inductors and capacitors connected in

Authorized licensed use limited to: Politecnico di Torino. Downloaded on January 15,2026 at 08:57:10 UTC from IEEE Xplore. Restrictions apply.
© 2025 IEEE. All rights reserved, including rights for text and data mining and training of artificial intelligence and similar technologies. Personal use is permitted, but republication/redistribution requires IEEE permission. See https://www.ieee.org/publications/rights/index.html for more information.

This article has been accepted for publication in IEEE Journal of Emerging and Selected Topics in Power Electronics. This is the author's version which has not been fully edited and content may change prior to final publication. Citation information: DOI 10.1109/JESTPE.2025.3584899



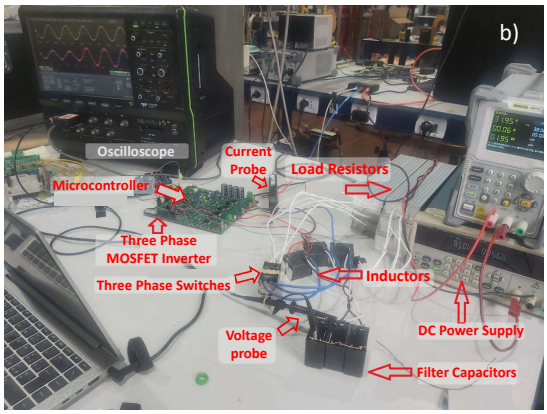


Fig. 10. a) Schematic block circuit of the inverter system and load used. b) Experimental setup.

parallel. The input voltage is given by connecting two voltage sources in series. Two pairs of three resistors, used as the load, are connected in parallel through a switch that is turned on or off to test the performance of the controller in real-time. The parameters of the setup and the values used for controller are as shown in Table I and Table II, respectively. The input voltage is fixed at 40 V, for a desired output peak voltage of 24 V phase to phase. The inductors used are 100 μH each with a saturation current of 9 A. Three film capacitors of 20 μF each were used. Initially, the load was fixed at 3.3 Ω. To test the validity of the controller, the load was varied by connecting another pair of 3.3 Ω loads in parallel, so when the switch is turned on, the load is halved to a value of 1.65 Ω. The three-phase MOSFET switches were operated at the frequency of 45 kHz to decrease the operational values of inductors required in the LC filter.

Initially, the controller was operated at the nominal values given in Table I. For a load of 3.3 Ω, with the converter operated at steady-state, Fig. 11 shows the waveforms for voltage and inductor current on the oscilloscope. It should be noted that for the ease of voltage sensor implementation, the voltage was sensed between the phase and neutral points. Hence, the voltage seen in these figures here is actually 24 V divided by $\sqrt{3}$. Moreover, voltages and currents in the oscilloscope waveforms are in phase.

As shown in Fig. 11, the voltage is tracked perfectly for the given reference value. The inductor current is in phase with the voltage. The slight perturbation in the voltage waveform at zero crossing is due to the dead time implemented in the operation of MOSFET switches to prevent leg short circuit.

The next step in the testing was to turn the switch on

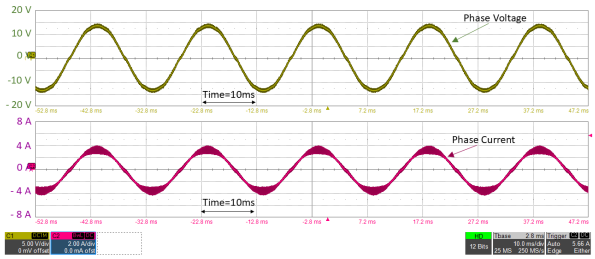


Fig. 11. Experimental waveforms of the inverter phase voltage (upper trace, green) and phase current (lower trace, purple) for the 3.3 Ω resistive load. V = 5 V/div, I = 2 A/div, t = 10 ms/div.

and monitor the performance of the controller when the load resistance is halved. The resulting oscilloscope waveform is shown in Fig. 12. The voltage remains constant, while the current is doubled.

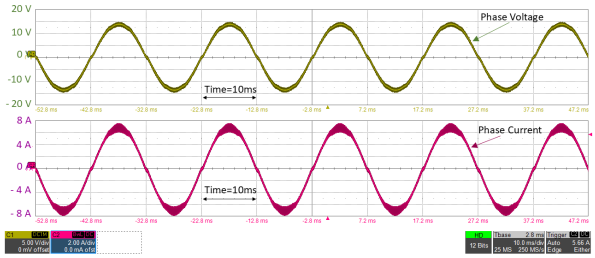


Fig. 12. Experimental waveforms of the inverter phase voltage (upper trace, green) and phase current (lower trace, purple) parallel resistive loads (1.65 Ω). V = 5 V/div, I = 2 A/div, t = 10 ms/div.

The most important part of the transition period is when the switch is turned on. To validate the performance of the controller with different target points, multiple screenshots of voltage and current waveforms were recorded at the instant of switching from 3.3 Ω load to 1.65 Ω load. The oscilloscope waveforms reported in Fig. 13 show cases with four different times when the switch was turned on. The results show that while the current was doubled each time, after a very fast transient the voltage remained constant for each case.

B. Comparison with Another Dual-loop PID Controller

To compare the results obtained for the regulation of inverter prototype, a dual-loop cascaded controller with an outer voltage loop and an inner current control loop has also been implemented. The control has been implemented in the rotating reference frame that is synchronous with the three-phase sinusoidal reference voltage at the load side. The bandwidths of the current loop and voltage loop have been set to 500 Hz and 50 Hz, respectively. To test its performance, again the linear load was stepped down from 3.3 Ω to 1.65 Ω. Fig. 14 shows the variations in the load voltage as shown in the oscilloscope.

Data was also collected in Matlab for calculation and analysis purposes. It was determined that there is no significant steady-state error in the response (same as for the proposed controller) but the voltage does take longer to reach the steady-state value (approximately 20 ms). Concerning the

Authorized licensed use limited to: Politecnico di Torino. Downloaded on January 15,2026 at 08:57:10 UTC from IEEE Xplore. Restrictions apply.
© 2025 IEEE. All rights reserved, including rights for text and data mining and training of artificial intelligence and similar technologies. Personal use is permitted, but republication/redistribution requires IEEE permission. See https://www.ieee.org/publications/rights/index.html for more information.

This article has been accepted for publication in IEEE Journal of Emerging and Selected Topics in Power Electronics. This is the author's version which has not been fully edited and content may change prior to final publication. Citation information: DOI 10.1109/JESTPE.2025.3584899

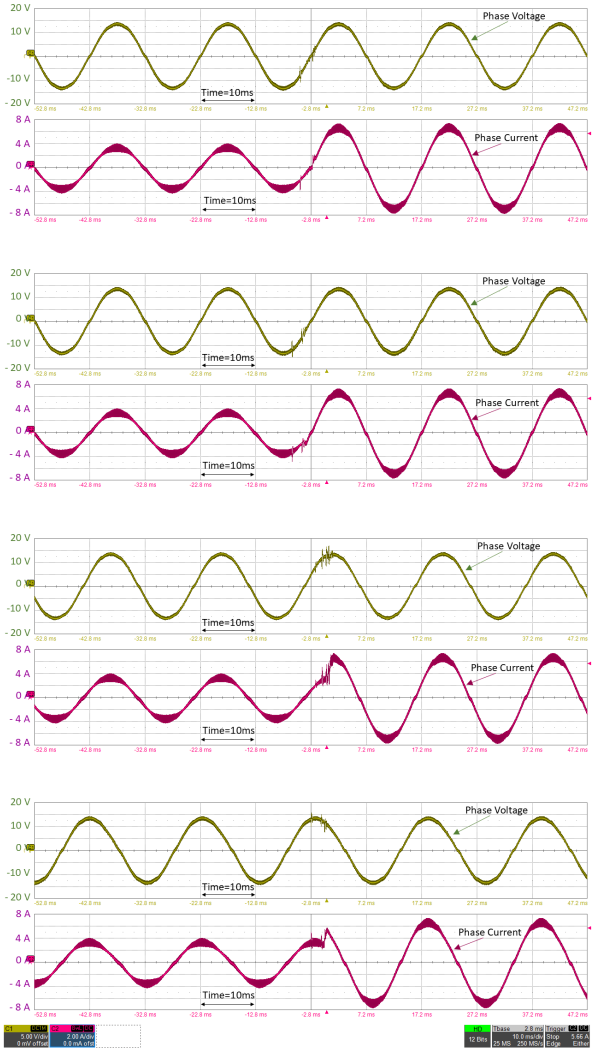


Fig. 13. Experimental waveforms of the inverter phase voltage (upper trace, green) and phase current (lower trace, purple) at different trigger points of the switch for load variation. V = 5 V/div, I = 2 A/div, t = 10 ms/div.

Total Harmonic Distortion, for the proposed controller the resulting THD% is 1.26%, while for the cascaded dual-loop controller the THD% is around 3.28%.

VI. Conclusion

In this paper, a novel TCB-based adaptive control approach has been proposed for a three-phase inverter. An observer has been designed to estimate the value of the load for reducing the number of sensors required to implement the control system. The proposed control architecture guarantees global stability of the closed loop system for both linear and nonlinear loads. The proposed approach shows negligible steady-state errors and low THD% for various load conditions. As the load increases, the THD% decreases to negligible values. Furthermore, the robustness of the proposed approach has been confirmed by varying the LC parameters, with low steady-state errors and low THD% even under high inductor and capacitor parametric uncertainties. All these characteristics

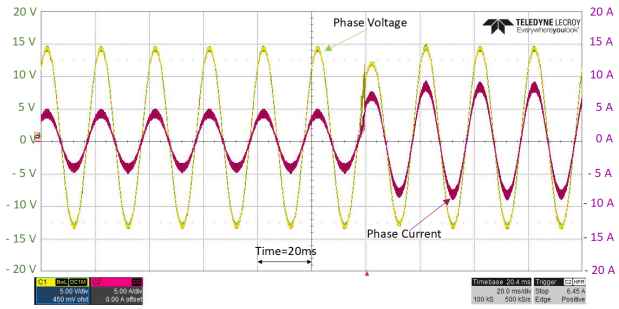


Fig. 14. Experimental waveforms of the inverter phase voltage (green trace) and phase current (purple trace) response of a cascaded dual-loop controller action at load variation. V = 5 V/div, I = 5 A/div, t = 20 ms/div.

confirm the proposed approach as a very effective alternative to the currently available solutions.

This paper has presented the fundamentals of the MRAC-TCB approach and the substantial results obtained with experimental confirmation on linear loads and steady-state output voltage reference. Further work is in progress to apply the proposed approach in various directions. While the computational paradigm remains the same, on the experimental side the applications under exam include the definition of reference trajectories based on predefined voltage transients, the extension of the experimental results to the use of unbalanced and nonlinear loads, and the operation of the proposed controller within three-phase inverters connected to the grid in different modes.

References

[1] S. Bayhan, S. S. Seyedalipour, H. Komurcugil, and H. Abu-Rub, "Lyapunov energy function based control method for three-phase UPS inverters with output voltage feedback loops," *IEEE Access*, vol. 7, pp. 113 699–113 711, August 2019.

[2] S. Kim, W. Chu, D. Raffo, D. Vo, and D. Patel, "Inverter improvement with SiC MOSFET for HVAC system," in *2024 IEEE Transp. Electrific. Conf. and Expo (ITEC)*. IEEE, June 2024, pp. 1–6.

[3] Y. Zhang and X. Ruan, "Three-phase AC–AC converter with controllable phase and amplitude," *IEEE Trans. Ind. Electron.*, vol. 62, no. 9, pp. 5689–5699, March 2015.

[4] R. Wu, S. B. Dewan, and G. R. Slemon, "Analysis of an AC-to-DC voltage source converter using PWM with phase and amplitude control," *IEEE Trans. Ind. Appl.*, vol. 27, no. 2, pp. 355–364, April 1991.

[5] M. Mohseni and S. M. Islam, "A new vector-based hysteresis current control scheme for three-phase PWM voltage-source inverters," *IEEE Trans. Power Electron.*, vol. 25, no. 9, pp. 2299–2309, September 2010.

[6] D. G. Holmes, R. Davoodnezhad, and B. P. McGrath, "An improved three-phase variable-band hysteresis current regulator," *IEEE Trans. Power Electron.*, vol. 28, no. 1, pp. 441–450, May 2012.

[7] Z. Song, C. Xia, and T. Liu, "Predictive current control of three-phase grid-connected converters with constant switching frequency for wind energy systems," *IEEE Trans. Ind. Electron.*, vol. 60, no. 6, pp. 2451–2464, October 2012.

[8] L. Estrada, N. Vazquez, J. Vaquero, C. Hernandez, J. Arau, and H. Huerta, "Finite control set–model predictive control based on sliding mode for bidirectional power inverter," *IEEE Trans. Energy Convers.*, vol. 36, no. 4, pp. 2814–2824, March 2021.

[9] M. Easley, S. Jain, M. Shadmand, and H. Abu-Rub, "Autonomous model predictive controlled smart inverter with proactive grid fault ride-through capability," *IEEE Trans. Energy Convers.*, vol. 35, no. 4, pp. 1825–1836, May 2020.

[10] H. T. Nguyen, J. Kim, and J.-W. Jung, "Improved model predictive control by robust prediction and stability-constrained finite states for three-phase inverters with an output LC filter," *IEEE Access*, vol. 7, pp. 12 673–12 685, January 2019.

Authorized licensed use limited to: Politecnico di Torino. Downloaded on January 15,2026 at 08:57:10 UTC from IEEE Xplore. Restrictions apply.
© 2025 IEEE. All rights reserved, including rights for text and data mining and training of artificial intelligence and similar technologies. Personal use is permitted, but republication/redistribution requires IEEE permission. See https://www.ieee.org/publications/rights/index.html for more information.

This article has been accepted for publication in IEEE Journal of Emerging and Selected Topics in Power Electronics. This is the author's version which has not been fully edited and content may change prior to final publication. Citation information: DOI 10.1109/JESTPE.2025.3584899

[11] P. Mattavelli, "An improved deadbeat control for UPS using disturbance observers," *IEEE Trans. Ind. Electron.*, vol. 52, no. 1, pp. 206–212, February 2005.
[12] M. Pichan, H. Rastegar, and M. Monfared, "Deadbeat control of the stand-alone four-leg inverter considering the effect of the neutral line inductor," *IEEE Trans. Ind. Electron.*, vol. 64, no. 4, pp. 2592–2601, November 2016.
[13] T.-S. Lee, K. Tzeng, and M. Chong, "Robust controller design for a single-phase UPS inverter using μ-synthesis," *IEE Proc.-Electr. Power Appl.*, vol. 151, no. 3, pp. 334–340, May 2004.
[14] D.-E. Kim and D.-C. Lee, "Feedback linearization control of three-phase UPS inverter systems," *IEEE Trans. Ind. Electron.*, vol. 57, no. 3, pp. 963–968, January 2010.
[15] O. Kukrer, H. Komurcugil, and A. Doganalp, "A three-level hysteresis function approach to the sliding-mode control of single-phase UPS inverters," *IEEE Trans. Ind. Electron.*, vol. 56, no. 9, pp. 3477–3486, March 2009.
[16] M. Pichan and H. Rastegar, "Sliding-mode control of four-leg inverter with fixed switching frequency for uninterruptible power supply applications," *IEEE Trans. Ind. Electron.*, vol. 64, no. 8, pp. 6805–6814, March 2017.
[17] H. Komurcugil and O. Kukrer, "Lyapunov-based control for three-phase PWM AC/DC voltage-source converters," *IEEE Trans. Power Electron.*, vol. 13, no. 5, pp. 801–813, September 1998.
[18] S. Rahmani, A. Hamadi, and K. Al-Haddad, "A Lyapunov-function-based control for a three-phase shunt hybrid active filter," *IEEE Trans. Ind. Electron.*, vol. 59, no. 3, pp. 1418–1429, August 2011.
[19] F. Torelli and A. Vaccaro, "A generalized computing paradigm based on artificial dynamic models for mathematical programming," *Soft Comput.*, vol. 18, pp. 1561–1573, August 2014.
[20] F. Torelli, A. Vaccaro, and N. Xie, "A novel optimal power flow formulation based on the Lyapunov theory," *IEEE Trans. Power Syst.*, vol. 28, pp. 4405–4415, June 2013.
[21] M. A. Qureshi, S. Musumeci, F. Torelli, A. Reatti, A. Mazza, and G. Chicco, "A novel model reference adaptive control approach investigation for power electronic converter applications," *Int. J. Electr. Power & Energy Syst.*, vol. 156, art. 109722, February 2024.
[22] S. Oucheriah and L. Guo, "PWM-based adaptive sliding-mode control for boost DC–DC converters," *IEEE Trans. Ind. Electron.*, vol. 60, no. 8, pp. 3291–3294, June 2012.
[23] R. F. Muktiadji, M. A. Ramli, H. R. Bouchekara, A. H. Milyani, M. Rawa, M. M. Seedahmed, and F. N. Budiman, "Control of boost converter using observer-based backstepping sliding mode control for DC microgrid," *Frontiers in Energy Res.*, vol. 10, art. 828978, March 2022.
[24] Z. Zhang and L. Xu, "Dead-time compensation of inverters considering snubber and parasitic capacitance," *IEEE Trans. Power. Electron.*, vol. 29, no. 6, pp. 3179–3187, June 2015.
[25] C. Lascu, "Sliding-mode direct-voltage control of voltage-source converters with LC filters for pulsed power loads," *IEEE Trans. Ind. Electron.*, vol. 68, no. 12, pp. 11 642–11 650, December 2020.
[26] Y. Qi, L. Peng, M. Chen, and Z. Huang, "Load disturbance suppression for voltage-controlled three-phase voltage source inverter with transformer," *IET Power Electron.*, vol. 7, no. 12, pp. 3147–3158, December 2014.
[27] P. Cortés, G. Ortiz, J. I. Yuz, J. Rodríguez, S. Vazquez, and L. G. Franquelo, "Model predictive control of an inverter with output *LC* filter for UPS applications," *IEEE Trans. Ind. Electron.*, vol. 56, no. 6, pp. 1875–1883, February 2009.
[28] J. He and X. Zhang, "A modified Lyapunov-based control scheme for a three-phase UPS with an optimal third-order load current observer," in *IEEE 10th Int. Symp. on Power Electron. for Distrib. Gener. Syst. (PEDG)*, August 2019, pp. 233–236.

Authorized licensed use limited to: Politecnico di Torino. Downloaded on January 15,2026 at 08:57:10 UTC from IEEE Xplore. Restrictions apply.
© 2025 IEEE. All rights reserved, including rights for text and data mining and training of artificial intelligence and similar technologies. Personal use is permitted, but republication/redistribution requires IEEE permission. See https://www.ieee.org/publications/rights/index.html for more information.